# DIAGNOSTIC METHODS OF SUPERCONDUCTING CAVITIES AND IDENTIFICATION OF PHENOMENA

H. Piel
University of Wuppertal
Federal Republic of Germany

## 1. INTRODUCTION

During the 197os a great number of diagnostic techniques applicable to superconducting rf cavities have been developed and refined in several laboratories. A variety of methods has been used to gain more insight into energy loss mechanisms additional to those which are always present when an rf field interacts with a superconducting surface. In order to review different diagnostic techniques it is useful to sketch a picture of the "inner life" of a cavity operated at high fields. Numerous experiments and theoretical analysis performed in the past have lead to the following ideas of the main energy loss processes [for a recent review see refs. 1,2].
Practically every superconducting cavity contains on its rf surface very small regions which are either normal conducting or become normal conducting at fields well below the bulk critical field of the superconductor. These weak spots can be present from the very beginning or they can be produced by impacting high intensity and high energy electrons during the operation of the cavity [3,4 ]. During the increase of the rf field these spots will produce an increasing heat flux which finally leads to a temperature increase of its surrounding above $T_c$ [5] or to the onset of film boiling on the cavities outside [4].

Both phenomena will give rise to a breakdown of the rf field (quenching). Multipacting, especially oneside multipacting has been identified as one of the most annoying field limiting effects in superconducting cavities [6]. This effect manifests itself by changes in the rf signal emitted by the cavity and by small areas of increased temperature on the cavity wall. Light emitting microparticles on the cavity surface have been observed in many instances [7,8]. They can emit electrons which heat up the cavity wall. The observation of rf field emitted electrons and their production of Bremsstrahlung when hitting the cavity wall has been with us since the first tests of low frequency ( < 3 GHz) cavities.

In my talk I want to review the diagnostic techniques which have been developed to identify and understand these phenomena and I also will try to correlate specific experimental observation with the particular energy loss process. I will however, restrict myself to those measurements which are performed on cavities under operating conditions at low temperatures.

In all experiments the rf signal emitted by the cavity, its amplitude and frequency as a function of the field level, bath temperature and time can be analysed. The second class of diagnostic techniques uses the intensity and the energy of the X-rays emitted from the cavity at high field levels. To this group of techniques I also want to add the observation of light emitted from the cavity interior and the measurement of free electron currents inside the resonator. The third and very important diagnostic method is the measurement of the temperature of the cavity wall. The importance of this method is evident from the fact that almost each energy loss mechanism will lead to an increase of the heat flux from the cavity to the surrounding helium bath. My talk will therefore be divided into three paragraphs.

## 2. THE "TELL TALE FEATURES OF THE RF-SIGNAL"

A test of a s.c. cavity is performed by applying a pulsed rf-signal ($U_i(t)$) to the cavity and observing the reflected signal ($U_r(t)$) and the signal transmitted by the cavity ($U_t(t)$). Frequency and amplitude of this signal contain the basic informations about the cavities response to the external rf-signal. Fig. 1 shows a schematic experimental set-up to analyse these signals.

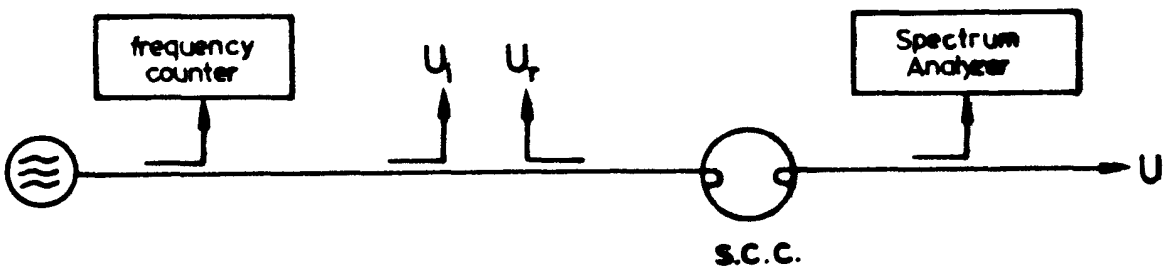


Fig.1:

Fig. 2 shows $U_i(t)$, $U_r(t)$ and $U_t(t)$ from an ideal s.c. cavity - generally measured at low field levels.

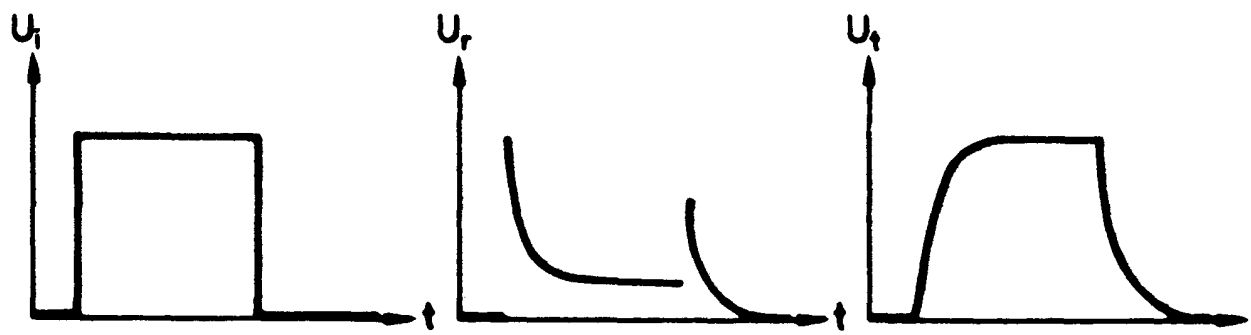


Fig. 2: $U_i(t)$, $U_r(t)$ from an ideal cavity

The amplitude and the decay times of these signals are used to determine the loaded Q of the cavity ($Q_L$) the coupling factor ($\beta$) to the rf driving network and the field level excited in the cavity i.e. the peak electric field $E_p$, the peak magnetic field $H_p$ or the effective accelerating field $E_a$. The unloaded cavity Q ($Q_o$) as a function of $E_p$ measured at different bath temperatures gives an integral measurement of loss mechanisms and their field dependence. As I want to concentrat on diagnostic techniques I will not discuss the different ways of analysing $Q_o(E)$ data. The observation of the times dependence of $U_t$ at different field levels will give additional informations and I will try to compile a catalogue of signals and their correspondence to specific energy loss phenomena.

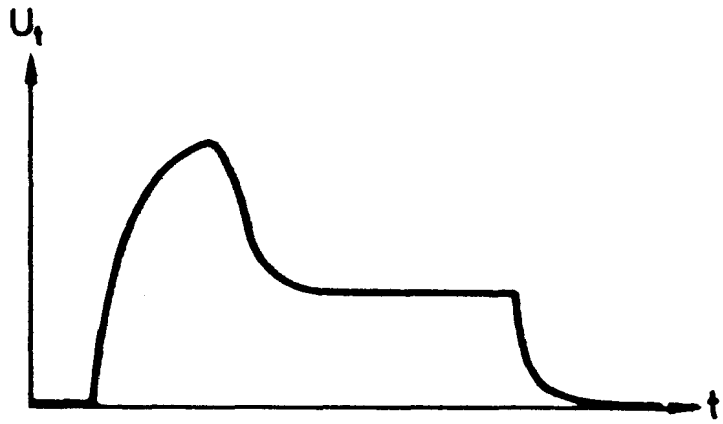


Fig. 3:

$U_t(t)$ from a cavity with high residual losses.

Fig. 3 shows $U_t$ from a cavity with a rf surface [see e.g. ref.9] of high residual resistance ($R_{res}$ > 1 $\mu\Omega$ typically). Already during the build up time of the field the temperature of the surface increases, Q deteriorates, $\beta$ reduces and the cavity stabilizes at a low field level. Another well known loss mechanism which can show up already at low field levels is electron multipacting.

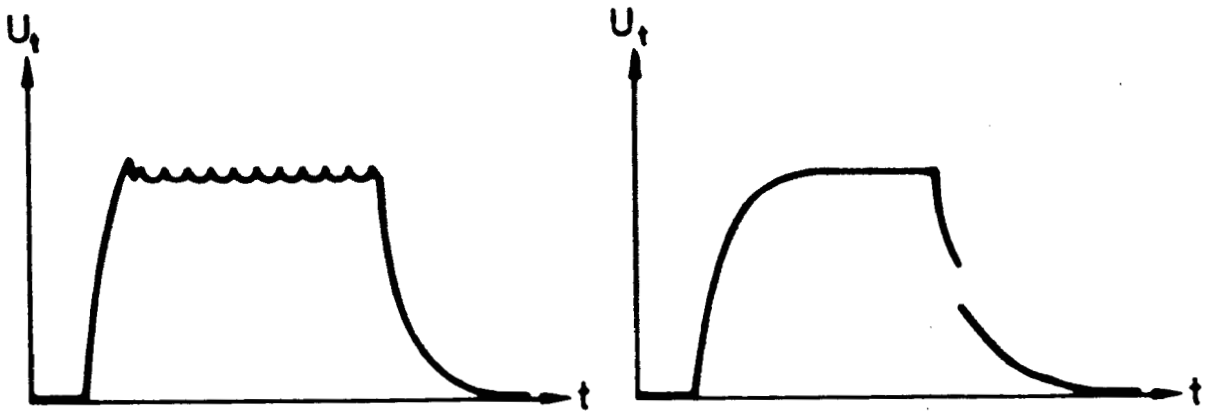


Fig. 4a: Fig. 4b:
Typical rf signals from a "multipacting cavity"

Fig. 4 shows characteristic $U_t$ signals at multipacting barriers [1o,11]. Multipacting will appear at very definite field levels (very high order multipacting can result in softer limitations). As the field rises one will fall (sometimes after a slight overshoot) into a multipacting threshold like shown in fig. 4a. A further increase of the rf power will not increase the field. At this level often processing is done to surmount the barrier by electron bombarding the small surface area responsible and thereby reducing the secondary emission $\delta$ coefficient below 1 [12]. By applying high power signals to the cavity a soft multipacting barrier ( $\delta$ close to 1 ) can be overcome due to the lack of time needed for its build up. Then frequently a signal like in fig. 4b is observed. The excessive energy loss by multipacting indicates itself during the slow decay of the rf field and very low Q jumps are observed in the decay slope. To identify multipacting the observation of the frequency of $U_t$ is valuable. Frequency changes of as much as 1o kHz have been observed in GHz-cavities [11]. The multipacting electrons can also give rise to the excitation of higher order modes in the cavities frequency spectrum [13].

If one succeeds to circumvent multipacting by an appropriate cavity geometry [14,15,16] or by electron processing one may come to higher electric fields where field emission becomes the next obstacle. Field emission loading is particularly observed in low frequency (large volume!) cavities and the $U_t$ signal looks like in fig. 5.

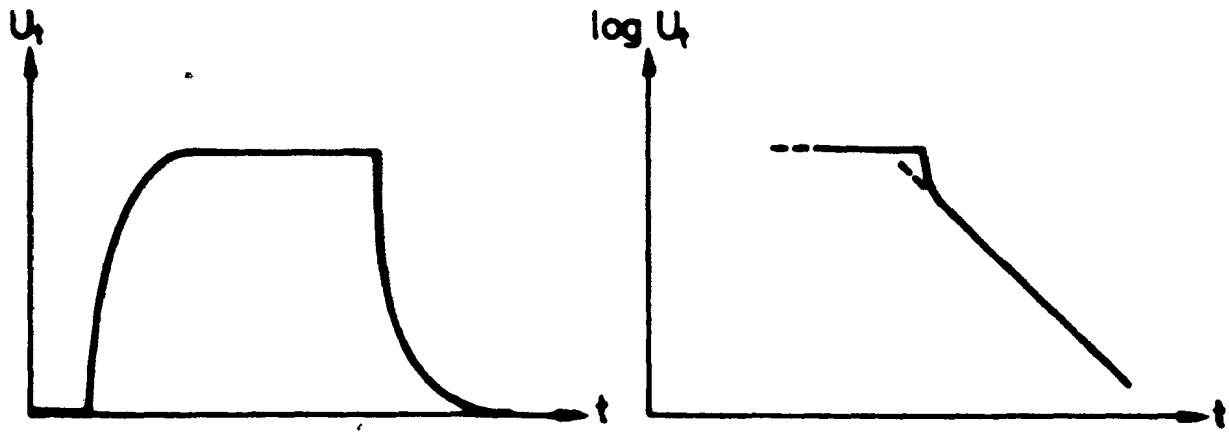


Fig. 5a Fig 5b

$U_t(t)$ and log $U_t(t)$ from a cavity with field emission loading

The presence of field emitted electrons can be seen from $U_t$ by the non-exponential decay. The use of a logarithmic amplifier makes this observation more evident. It is important to use such an amplifier to analyse $U_t$ because a non-exponential decay can be overseen quite easily and may lead to significant errors in the determination of the achieved Q- and field levels.

In the presence of strong electron currents in the cavity either caused by multipacting or by field emission higher eigenfrequencies of the cavity , the so called higher order modes,can be excited. $U_t(t)$ then shows a time dependence like in fig. 6.

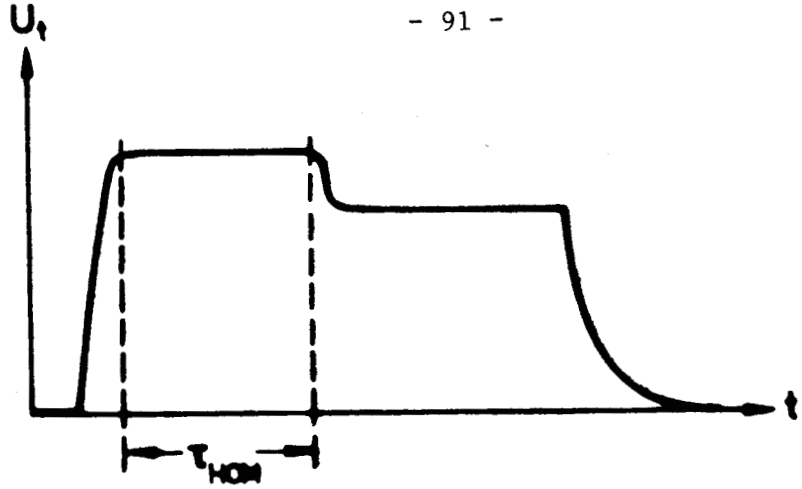


Fig. 6: Higher order mode excitation

Some time after the excitation of the fundamental mode a higher cavity mode is excited by the free electrons which act as coupling currents. This delay time $\tau_{HOM}$ is generally one or two orders of magnitude longer than the unloaded decay time of the fundamental mode and decreases with increasing internal currents. This HOM excitation has been observed at Stanford [13] and at CERN [4]. Most higher order modes don't couple as well to the rf probe as the fundamental mode. Therefore, once the higher mode is excited $U_t$ decreases. If HOM's of high frequencies are excited this picture however can change and $U_t$ may show an increase after $\tau_{HOM}$. If there is a suspicion of HOM excitation a spectrum analyser is a very useful tool and $U_t$ should only be used as a first indication.

In practice all superconducting cavities, also those which are apparently free of electron loading phenomena (f > 1o GHz), will have some surface imperfections which are often classified as weak spots and which are assumed to be of microscopic size [5]. Such weak spots may be normal conducting or superconducting but with a low critical field and (or) a low critical temperature compared to the parameters of the bulk material . Superconducting weak spots have been observed in recent CERN experiments and can show up in the $U_t$ signal at the field level

of their phase transition. At this field a new loss mechanism is switched on and a sudden change in the cavity Q results which leads to a $U_t$-signal like shown in fig. 7.

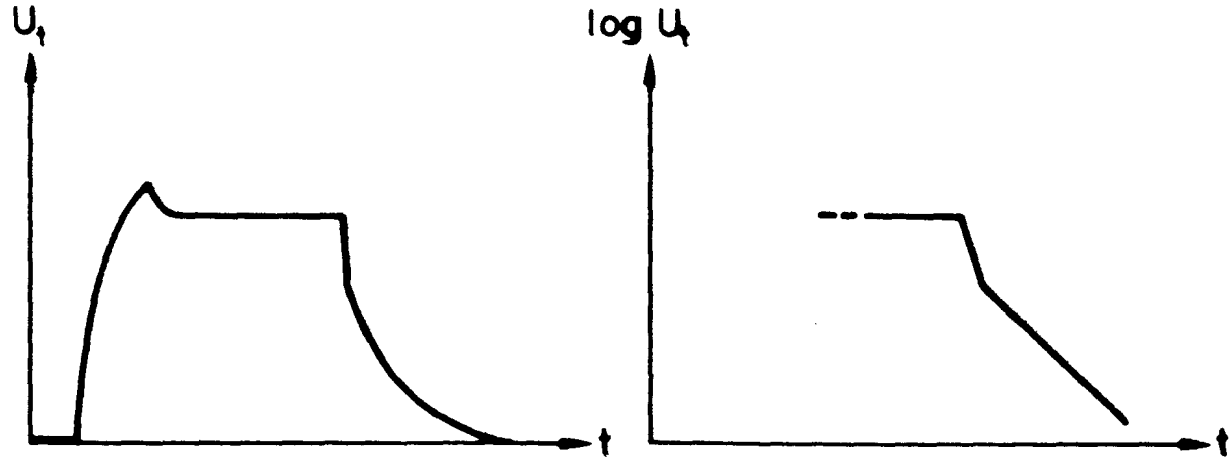


Fig. 7a Fig. 7b
Phase transition of a weak spot

This signal can be mistaken for a multipacting signal (fig. 4a) however, one can increase $U_t$ easily by applying more rf-power to the cavity. If one then observes the decay of $U_t$ with a logarithmic amplifier, one will observe a kink in the decay slope, corresponding to two Q-values. We know that weak spots of this nature can be attributed to a surface damage caused by impacting high energy and high intensity field emitted electrons.

If not limited by electron loading the cavity field will be finally limited by a quenching phenomena induced by the described weak spots. The high heat flux density produced by these areas will either drive their environment on the rf surface normal and lead to an unstable state or the film boiling limit on the outside of the cavity wall will be exceeded. Both phenomena will lead to a sudden dissipation of the energy stored in the cavity at a fixed field level - the "quench field". This limitation often described as "magneto thermal" breakdown will lead to a $U_t$ signal

like shown in fig. 8.

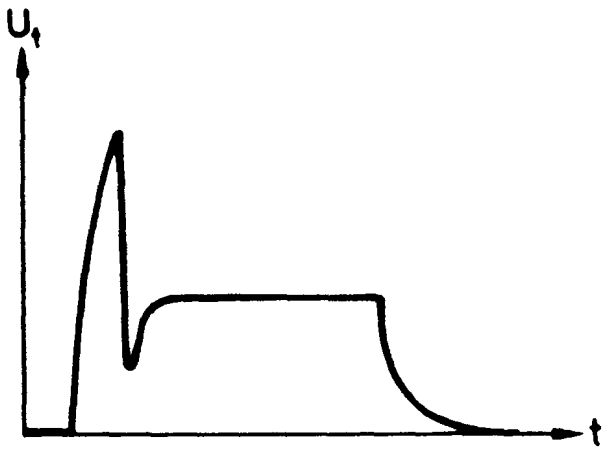


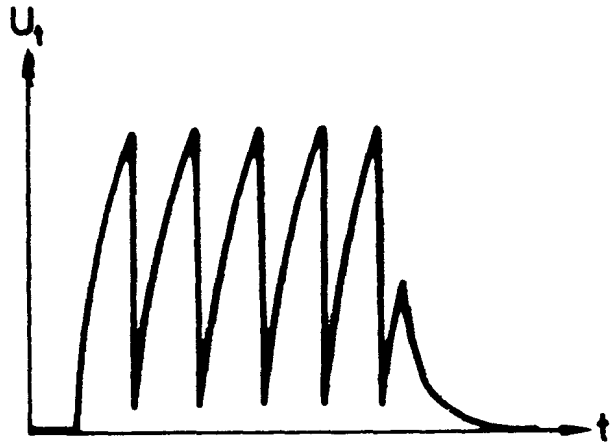


Fig. 8a

Fig. 8b

Rf-breakdown - quenching

If a single quench like in fig. 8a or a self-pulsing quench like in fig. 8b will result depends on the cooling conditions, the coupling factor $\beta$ and the cavities Q. The quench time $\tau_q$ is in general one or two orders of magnitude below the characteristic decay time $\tau$ of the undisturbed cavity. In cavities with poor vacuum an rf breakdown by gas discharge is possible. $U_t$ will then be very similar to fig. 8b, however, in general at much lower field levels.

Impacting electrons from field emission or multipacting or a changed surface heating by an excited higher order mode can also lead to an excessive heat flux into a small surface area. Therefore, the $U_t$ signals of fig. 8 can show up combined with those of fig. 4,5 or 6.

In conclusion of this chapter one can say that all known Q and field limiting phenomena can be observed by a careful analysis of the rf signal emitted by the cavity. To do this the "diode signal" should not only be observed directly but also via a logarithimic amplifier. Aside of the frequency counter, generally used in a cavity experiment, a spectrum analyser can reveal valuable informations about higher order mode excitations.

## 3. DETECTION OF X-RAYS, ELECTRONS AND LIGHT

The observation of the cavities rf signal is an excellent diagnostic tool in order to see if one is in trouble. It will also tell what kind of limiting mechanism is present. A more detailed analysis of the problems cause however needs additional experimental information. Right from the beginning of the work with low frequency (large volume) cavities X-radiation was detected. X-ray intensities are monitored using essentially four different instrumentations: Ionisation chambers, NaJ-crystal detectors - with [17] and without collimation, pin hole X-ray cameras [18] and scanning surface barrier detectors close to the cavity wall [4]. The first three detectors are used outside the cavity cryostat and the latter inside the helium bath. Ionisation chambers and NaJ detectors are used to measure the intensity of the Röntgen radiation and their dependence on the peak electric surface field. The X-ray intensity increases exponentially with increasing field and is analysed using the Fowler-Nordheim relation [19]. The methods involved will be discussed in the report of C. Lyneis. With NaJ detectors not only intensity but also the energy of the emitted X-rays can be measured. The determination of the maximum energy of the observed Bremsstrahlenspectrum gives information about the internal electron trajectories. The measurement of the spatial distribution of the X-radiation also is used for this purpose. The measurements may be used to determine location and distribution of electron emitting sources if used in combination with trajectory calculations. Recently at Karlsruhe an experiment was performed with a 7oo MHz TM-like cavity, where X-ray spectra have been taken together with the X-ray intensity distribution along the cavity wall [17]. A NaJ-detector together with a collimator was used and the experimental set-up is shown in fig. 9. Figs. 1o shows some typical results of the measured spatial and energy distribution The emission of high

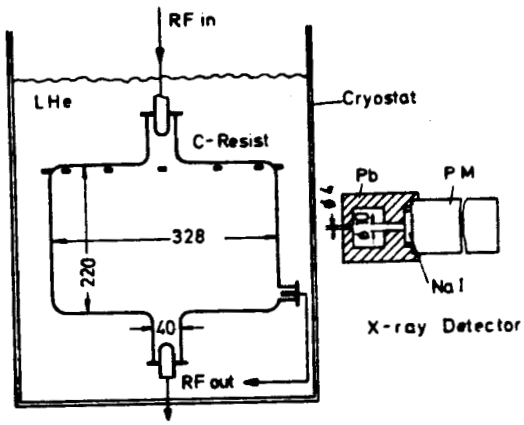


Fig. 9: Sketch of the experimental set-up of the Karlsruhe 7oo MHz cavity [17]

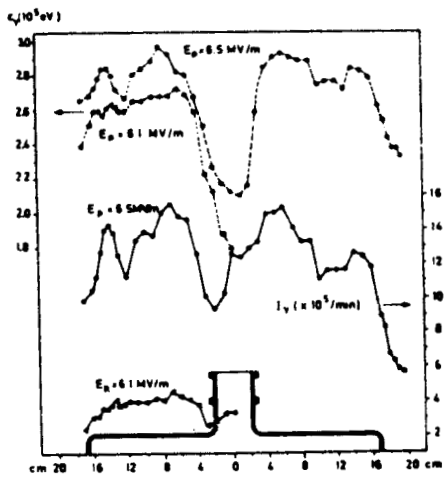

Fig. 1o: X-ray distribution in intensity $I_\gamma$ and energy $\varepsilon_\gamma$ at the endplate of the Karlsruhe 7oo MHz cavity at a field level $E_p$ = 6.1 and 6.5 MV/m [17]

energy X-rays is concentrated on the top and bottom plate of the cavity. Those data point to field emitted electrons and the importance of secondary processes which smear out the effect of several point like sources expected to be responsible for electron field emission. An information of the same nature has been obtained already in 1973 by X-ray photography of a L-band cavity operated at high fields at Stanford, where a pin hole camera together with an image amplifier was used [18]. The experimental set-up used is given in fig. 11 and one of the beautiful pictures is shown in fig. 12.

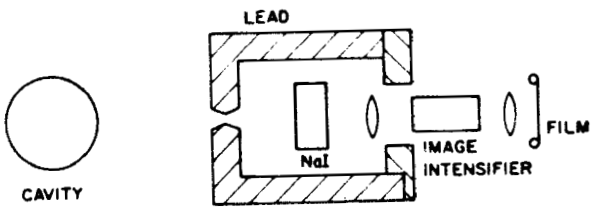


Fig. 11: Components of the Stanford X-ray camera

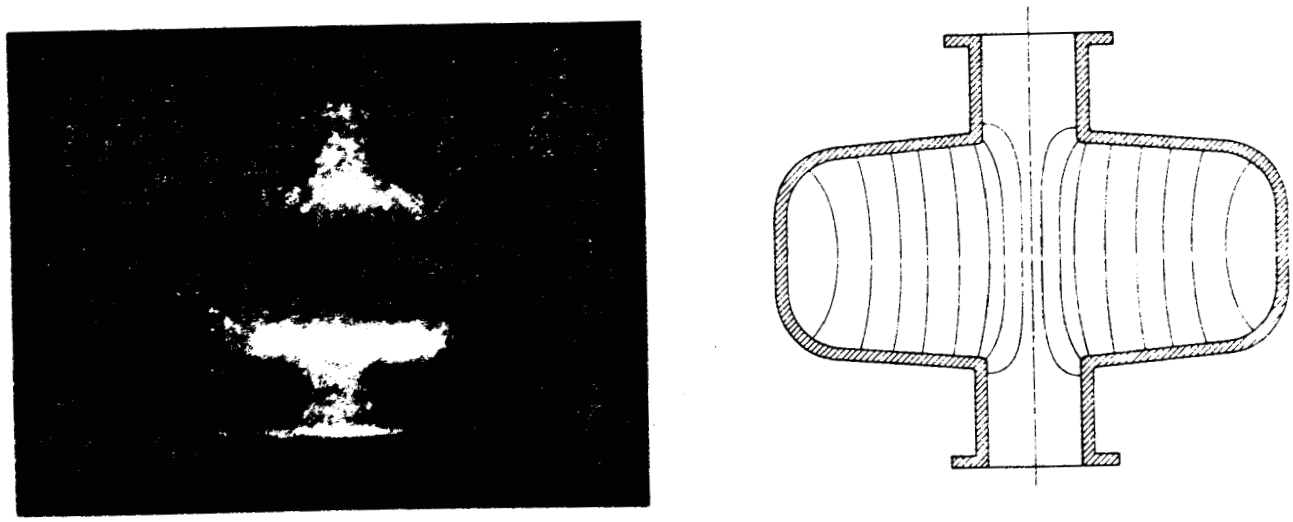

Fig. 12: X-ray-photography and crossectional view of the Stanford L-band cavity

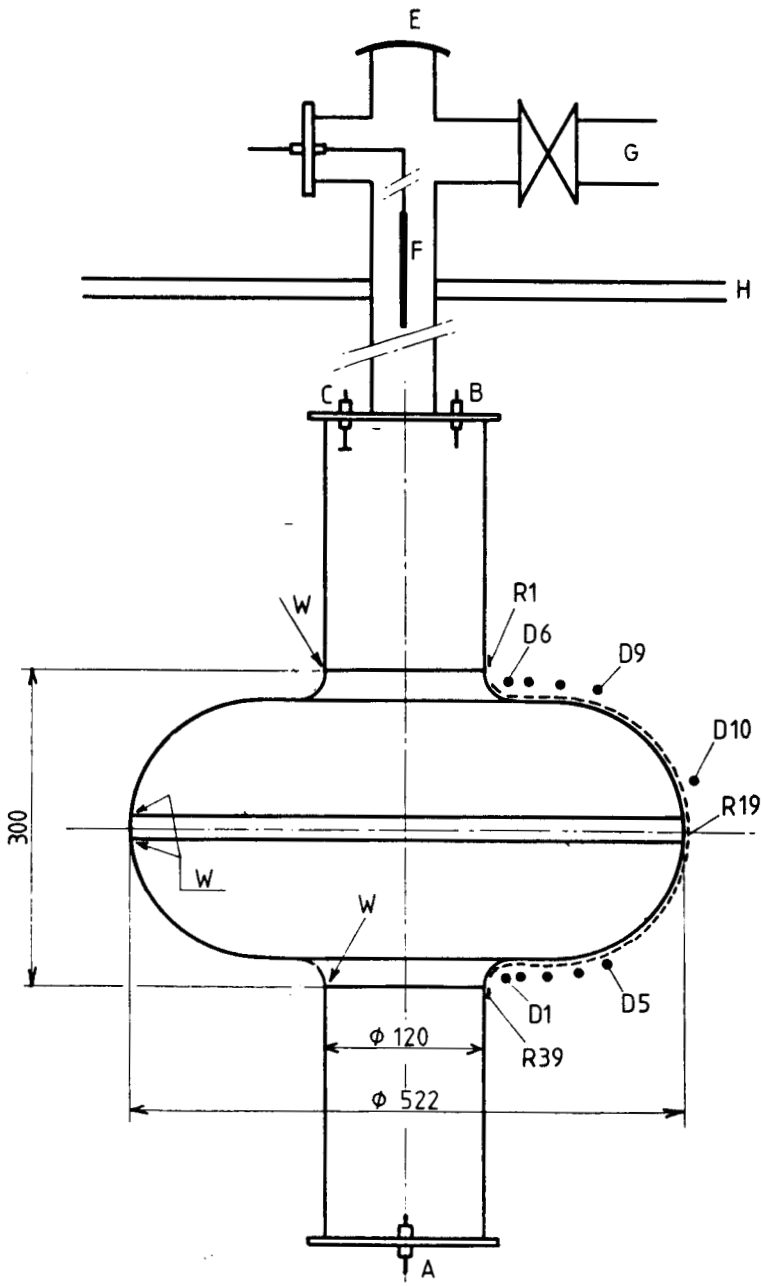


Fig. 13: Sketch of the CERN 5oo MHz cavity [ 4 ]
A,B,C = rf probes; E = viewing part;
F = retractable electrode for glow discharge cleaning; R1-R39 = scanning carbon thermometers;
D1-D1o scanning X-ray detectors; W = weld

A simple minded picture of field emission would start from a single (or a few) field emitting sources. The electrons from this source would move in one place and hitting the cavity wall would produce a line like X-rax source. One would therefore expect a strong azimuthal peaking of the X-radiation. This is not observed with both described techniques and one has to conclude that secondary multiplication processes play an important role. This is confirmed by the observed X-ray energies which only can be explained by a twostep process [18]. Some light on this problem is also shed by an experiment done a few weeks ago at CERN which uses ten scanning X-ray detectors on a 5oo MHz single cell cavity like shown in fig. 13. The solid state silicon detectors used (RT 1 Radiation Transducer, Quantrad Corporation, 2261 South Carmelina Avenue, Los Angeles) have a sensitive surface of 6 mm diameter and a sensitive thickness of 1ooμ. They are used in a charge sensitive mode as "solid state ionisation chambers". Fig. 14 shows plots of X-ray intensities measured with these detectors in different locations as a function of the azimuthal angle. X-ray emission peaked along one meridian of the cavity is clearly observed. At the bottom part of the cavity the X-ray sources are distributed along a very narrow line on top of broad almost uniform distribution. At the equator the intensity is low and uniform in distribution. At the top part of the cavity a very broad distribution is observed. This X-ray distribution has yet to be analysed by trajectory calculation including multiplication processes like in ref. 18. It appears to be likely however that the narrow part of the distribution is caused by the impact of primary electrons field emitted by a point source, whereas the broad distribution at the top of the cavity may be explained by secondary electrons which can gain higher energies in the

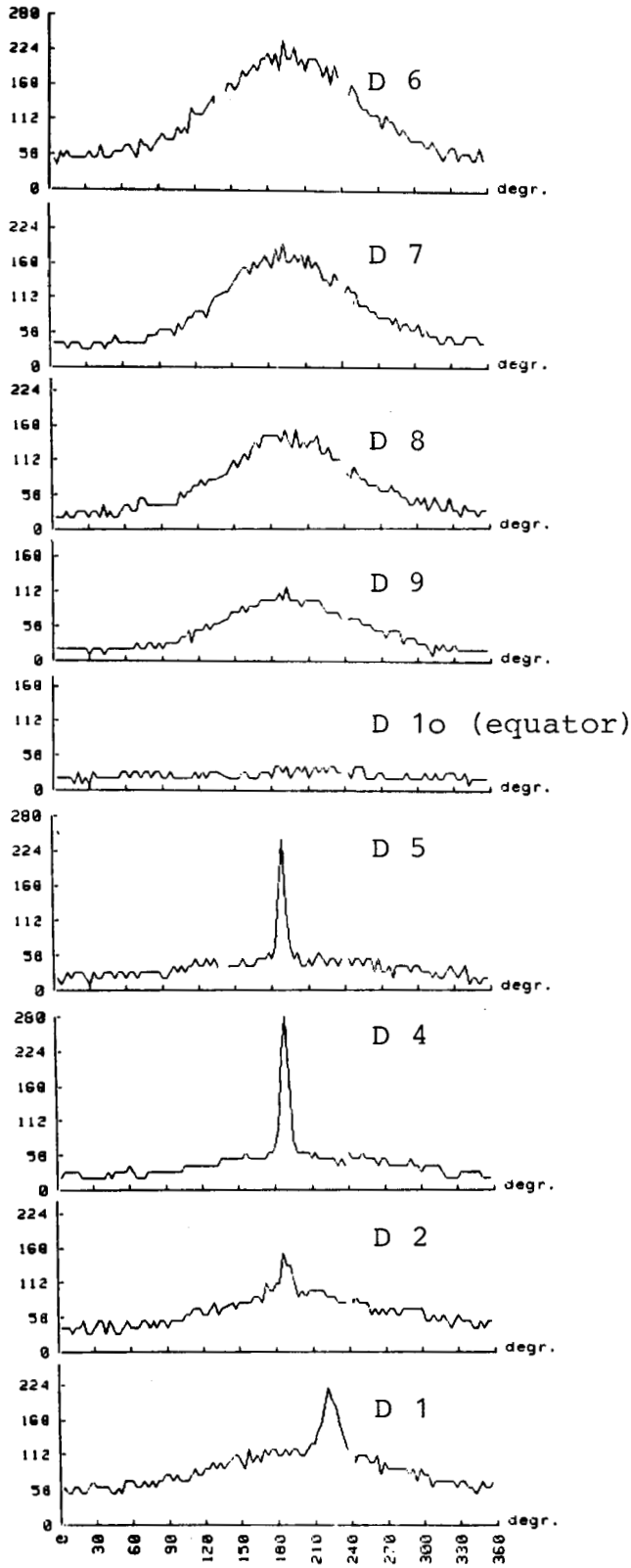


Fig. 14: Spatial distribution of X-ray intensity measured with the CERN 5oo MHz cavity at $E_a$ = 3.4 MV/m
Vertical axis: X-ray intensity in relative units
Horizontal axis: azimuthal position in degrees.

cavity field than the primary ones. The integrated X-ray intensity from the upper part of the cavity is considerably higher than the one from the peak dominated lower part. According to first trajectory calculations [2o] the photon energy in the peak region is considerably lower than the one of the X-rays coming from the top of the cavity. The shielding by the cryostat may therefore eliminate the sharp spikes in the X-ray distribution. Taking this into account and also assuming several field emitting sources at high fields, the Karlsruhe and Stanford X-ray intensity distributions do not contradict the ones of CERN.

In high frequency cavities or in cavities where the mean free path of an electron is to short, X-ray emission cannot be expected even under the presence of strong field emitting sources. In such cases internal electron probes, like shown in fig. 9 are very useful diagnostic tools (see also ref. 7 ). They will indicate the relative strength of the internal electron currents by picking up low energy secondary electrons. Bias voltages will depend on the special geometry of the probe and the cavity and range between +5o V and + 1oo V [17,21]. Also one is at present not able to determine the collection efficiency of such a probe it is observed that the measured electron currents follow quite accurately a Fowler-Nordheim relation and result in very similar local field enhancement factors compared to those from X-ray intensity measurements which in low frequency cavities are done simultaneously [see e.g. ref. 17].
In most experiments the rf couplers are used simultaneaously as electron probes.

Glowing micro particles (dust) have been seen in some instances [7,8 ] and have been considered to be

responsible for glow emission of electrons. It is therefore useful to have an optical window to inspect at least parts of the cavities' surface during high field operation. Mounting of a cavity in a "dust-free" environment can eliminate such glow emitters [8]. Also processing at high field levels can destroy these sources [7]. The current emitted glow emission unfortunately follows an exponential relation quite similar to the Fowler-Nordheim law and one may have to consider rf field emission from a hot microscopic particle [28]. Optical inspection can help to distinguish field and glow emission. Optical devices to view a large portion of the cavities' rf-surface during high field operation are therefore in preparation [22].

## 4. TEMPERATURE MEASUREMENTS

As each energy loss mechanism will finally lead to an increase of the temperature of the cavity wall, temperature measurements are of prime importance to identify causes for field and Q-limitations. C. Lyneis at Stanford was in 1972 the first to use a chain of rotating carbon resistors mounted in a few millimeter distance from a cavity wall to detect the location of a quench area [23]. Fig. 15 shows the first published oscilloscope trace of a heat puls detected by a carbon resistor close to quench area.

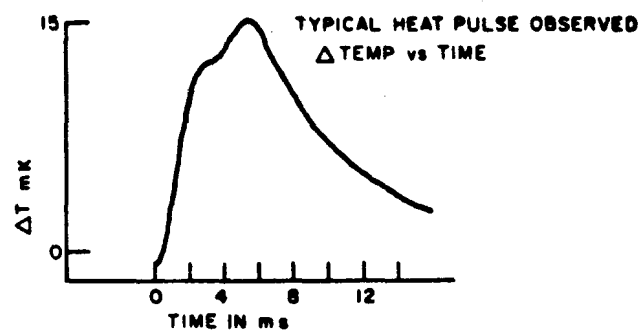


Fig. 15: "Typical heat pulse observed by a carbon resistor located a few millimeters from point of thermal magnetic breakdown"[5].

This method has been used thereafter by many groups working in this field (see e.g. ref. 24). The carbon thermometers used are 56 or 1oo Ω (1/8 W or 1/4 W) Allen Bradley resistors, the bakelite insulation of which is often grinded off to increase their sensitivity. Different electronic schemes have been used to readout the resistance value of the many thermometers generally used on one cavity [24,25] either using an oscilloscope display or an automatic data aquisition system. During a quench all the energy stored in a cavity is set free and a substantial heatflux develops which leads to film boiling and a marked increase of the temperature of the helium film close to the quench area. This can be detected easily even in superfluid helium and also if the resistor is not in contact to the cavity wall.

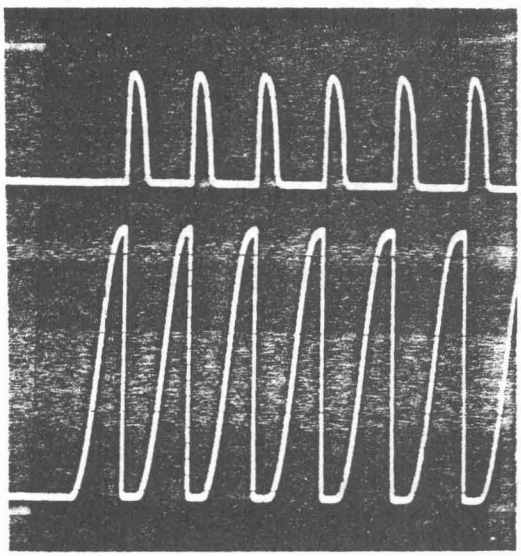

Fig. 16: Heat pulses (upper trace) associated with a self pulsing breakdown (lower trace) observed in the CERN 5oo MHz cavity [4] for $T < T_\lambda$.

Fig. 16 shows heat pulses associated with a self pulsing breakdown. The time duration of these heat pulses is typical in the millisecond region and their amplitude varies between 15 mK and 1.4 K depending on the helium bath

condition, the energy stored in the cavity and the distance of the resistor from the breakdown location. Using this technique quenches induced by multipacting electrons, which can change their location from rf puls to rf puls, have been discriminated from breakdown triggered by permanent surface damages and thereby preferred areas for electron multipacting have been identified [33]. Several experiments [e.g. 4,23] have shown a preference for quench areas in the bottom part of a cavity. This part of the cavity in general is not cooled as well, it is also the part which collects "falling dust" it will be cooled first and therefore residual gas in the cavity will be condensed first in this region. Whatever else may be the reason for the quenching preference is not yet clear.

Quenches especially in multicell structures deposit so much energy into the helium bath that second-sound waves can be detected. At Stanford several resistor rings are placed around the accelerating structure to pick up second-sound in order to localize the specific cell in which the breakdown occurs [13]. In Argonne second-sound waves from quenches in a split ring resonator are detected by single crystal germanium resistance thermometers [26]. The oscilloscope trace of fig.17 shows a second-sound signal initiated by a breakdown in a split ring resonator [27]. Using an array of typical 15 germanium thermometers one can reconstruct the location of the surface damage within 1 or 2 cm (speed of second-sound at $T < 2.1$ K: ≈20 m/s).

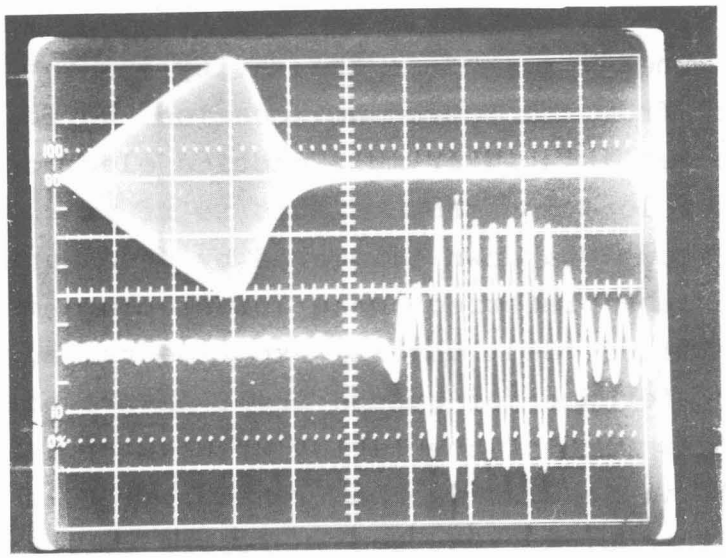

Fig. 17: " Oscilloscope display of the second-sound pulse associated with thermal breakdown of a resonator. The upper trace displays the rf field in the resonator, which is driven to $E_a$ = 3 mV/m at which point the resonator becomes thermally unstable and the field collapses. The lower trace displays the temperature of a sensor which shows a second-sound pulse arriving 13 msec after breakdown." [27]

At this point although not connected to thermometry another method to localize a "bad cell" in a multicell structure shall be mentioned. In the Karlsruhe - CERN - Separator [28] a poor cell was localized by measuring the resonators' Q as a function of the mode excitation. The knowledge of the field distribution of all resonator modes is necessary for the application of this diagnostic technique. In the separator tests also carbon thermometers were used to detect bubbles rising from the quench area. (With a speed of approximately 16 cm/s). Quench areas can be detected by their "bubble production" also by visual inspection, therefore, a cryostat window and an internal illumination can be quite useful[28]. The detection of quench areas is certainly a most useful diagnostic procedure. A temperature map of the surface of a cavity well below the

breakdown field however, will reveal even more information about the nature of high loss areas. Experiments on S-band muffin tin structures done at Cornell [24] and measurements of surface temperatures with germanium thermometers in Argonne [26] point into that direction. Temperature mapping can only be done for bath temperatures above the $\lambda$ temperature. The main obstacle for a temperature mapping experiment is the fact that only the temperature of the outside of the cavity wall can be measured which is very effectively cooled by the surrounding liquid helium. In a recent experiment at CERN [25] it was shown that temperature mapping can be carried out quite well in a subcooled helium bath (favourable subcooled condition: bath temperature slightly above $T_\lambda$ and bath pressure ≈ 1000mb). In a subcooled bath bubbles are absent and therefore the micro convection produced by bubbles rising from the heated surface is switched off. This reduces the cooling capability of liquid helium substantially and increases the heat transfer resistance between the niobium surface and the helium. Also the carbon thermometer which has to be in thermal contact to the cavity (fig. 18) is decoupled stronger from the cooling liquid. In a test experiment a weak spot on a 2 mm thick niobium wall was simulated by a heating resistor (fig. 19).

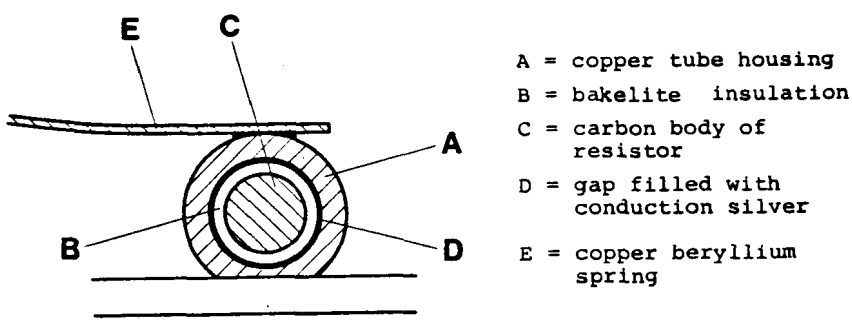


Fig. 18: Cross section through the carbon thermometer

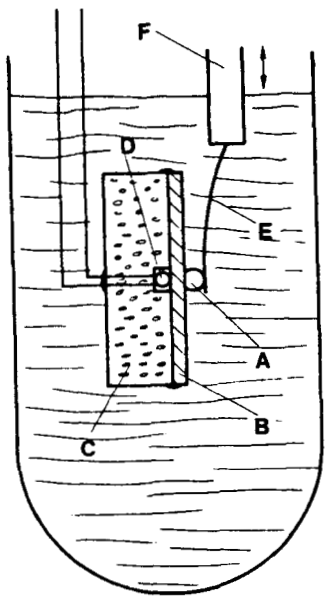


Fig. 19:

Set-up for testing a carbon thermometer

A = carbon thermometer
B = niobium sheet metal
C = styrofoam insulation
D = heating resistor
E = copper beryllium spring
F = movable rod

In fig. 2o the temperature distribution around this "simulated weak spot" is shown. It can be localized within ± 3 mm. The temperature increase $\Delta T$ on the outside wall was also measured as a function of the power $P_H$ applied to the heating resistor. The resulting data are shown in fig. 21. The observable heatflux and the corresponding temperature increases range over almost four decades. The set-up used for the temperature mapping of a 5oo MHz spherical cavity is shown schematically in fig.13 and in the photographs of fig. 22.

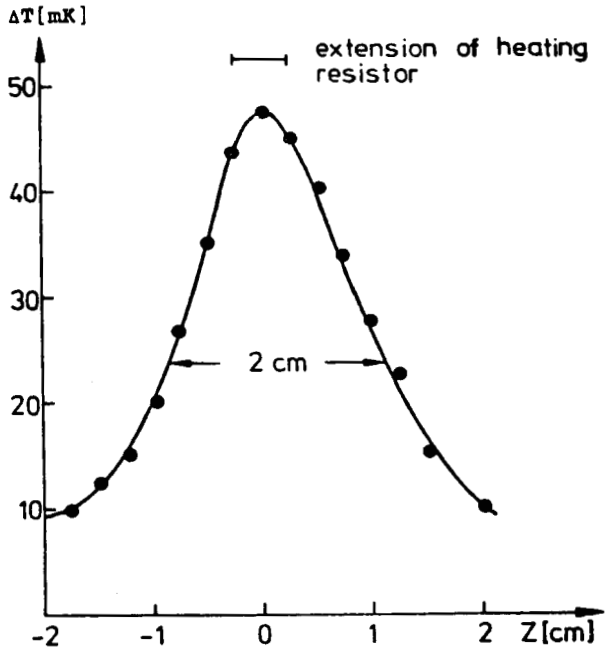


Fig. 2o:

Temperature distribution around the location of the heating resistor placed at z=o

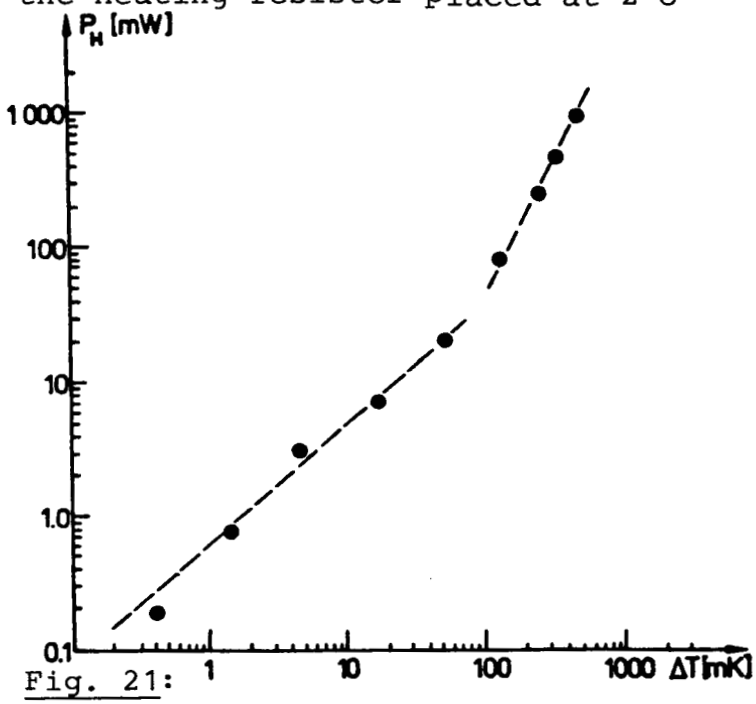


Fig. 21:

Temperature increase ΔT of the niobium wall (fig.19) and related heating power $P_H$ of the resistor.

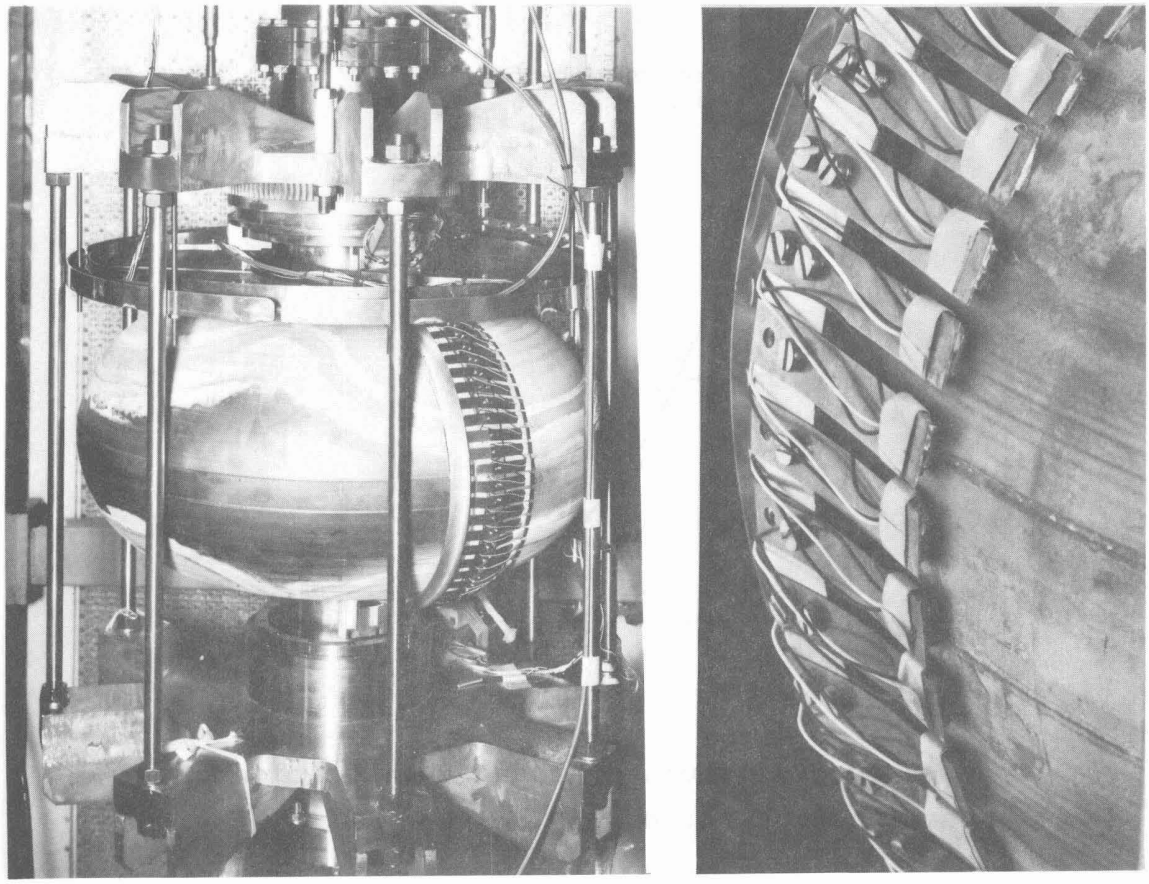

Fig. 22: General configuration and close up view of the carbon thermometer scanning system.

39 carbon thermometers (1oo Ω, 1/4 W Allen Bradley) are gliding under spring tension on the cavity wall and can be turned all around the cavity. The resistor voltages and their angular position are read by a computer controlled data acquisition system.[3o] Fig. 23 shows a 3 dimensional temperature map of the superconducting 5oo MHz niobium cavity operated at an effective accelerating field of 3.2 MV/m. This measurement was done in a subcooled helium bath at a temperature of 2.3 K. On the x-axis the distance along one circle of constant latitude around the spherical cavity is plotted. The y-axis shows the number of carbon thermometer (with resistor 1 corresponding to the top of the cavity and resistor 39 to the bottom of the resonator). The vertical axis displays the temperature increase $\Delta T$ detected by the carbon resistor. The residual resistance of this cavity was rather poor ($R_{res} \simeq$ 33o nΩ). It can be attributed to the very non-uniform high loss area at the

cavity top. The observed top to bottom assymmetry compared with other tests showed up problems in the procedure of the chemical treatment of the cavity.

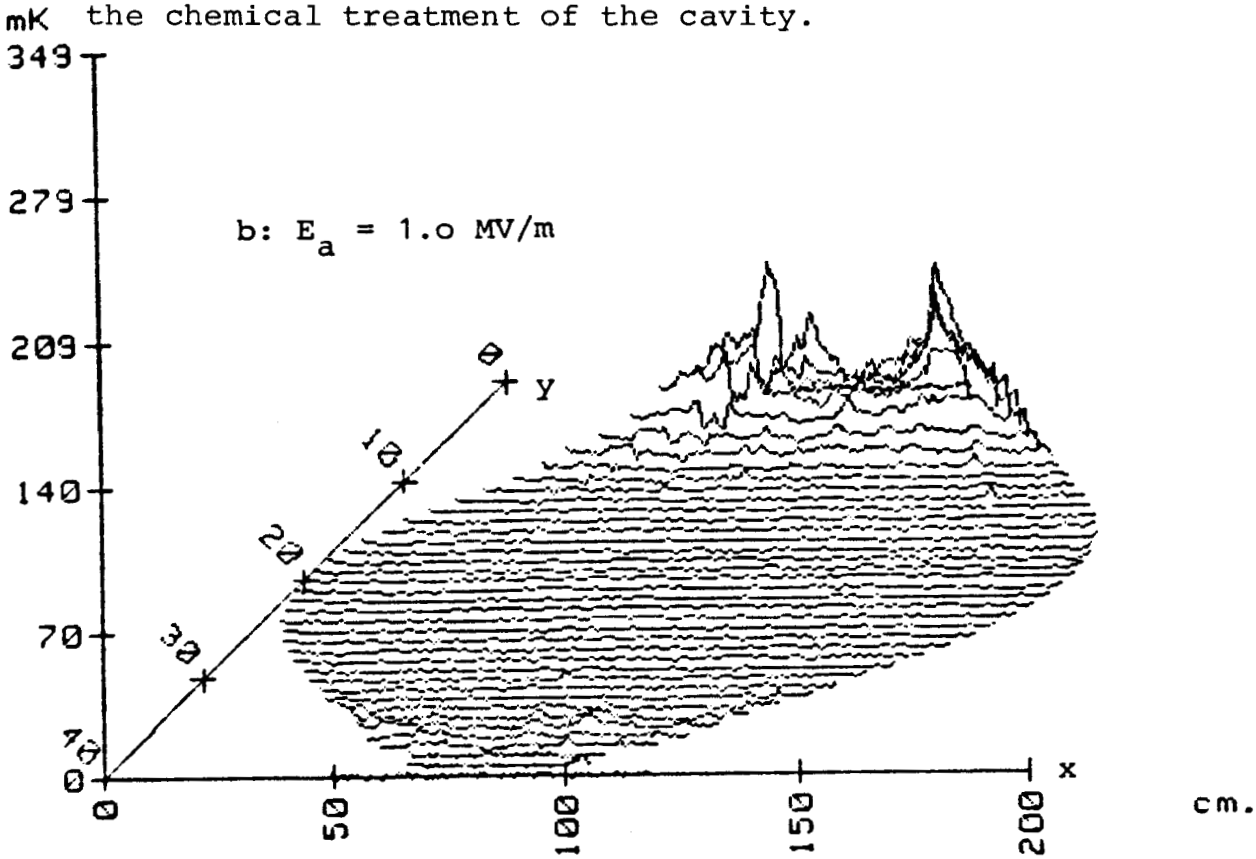


Fig. 23: Temperature map of the CERN 5oo MHz cavity at an accelerating field of 1.o MV/m

In fig. 24 typical temperature profile of the upper part of the cavity is plotted, measured by thermometer 4 along its path around the resonator for three different field excitations. By measuring such a profile in two successive scans but with otherwise identical conditions one can test the reproducibility of the temperature measurement. It is within stepping accuracy ($3^{o}$ in the shown data) for finding the location of the observed temperature peaks and the absolute value of the temperature is remeasured with deviations of less than 2o%.

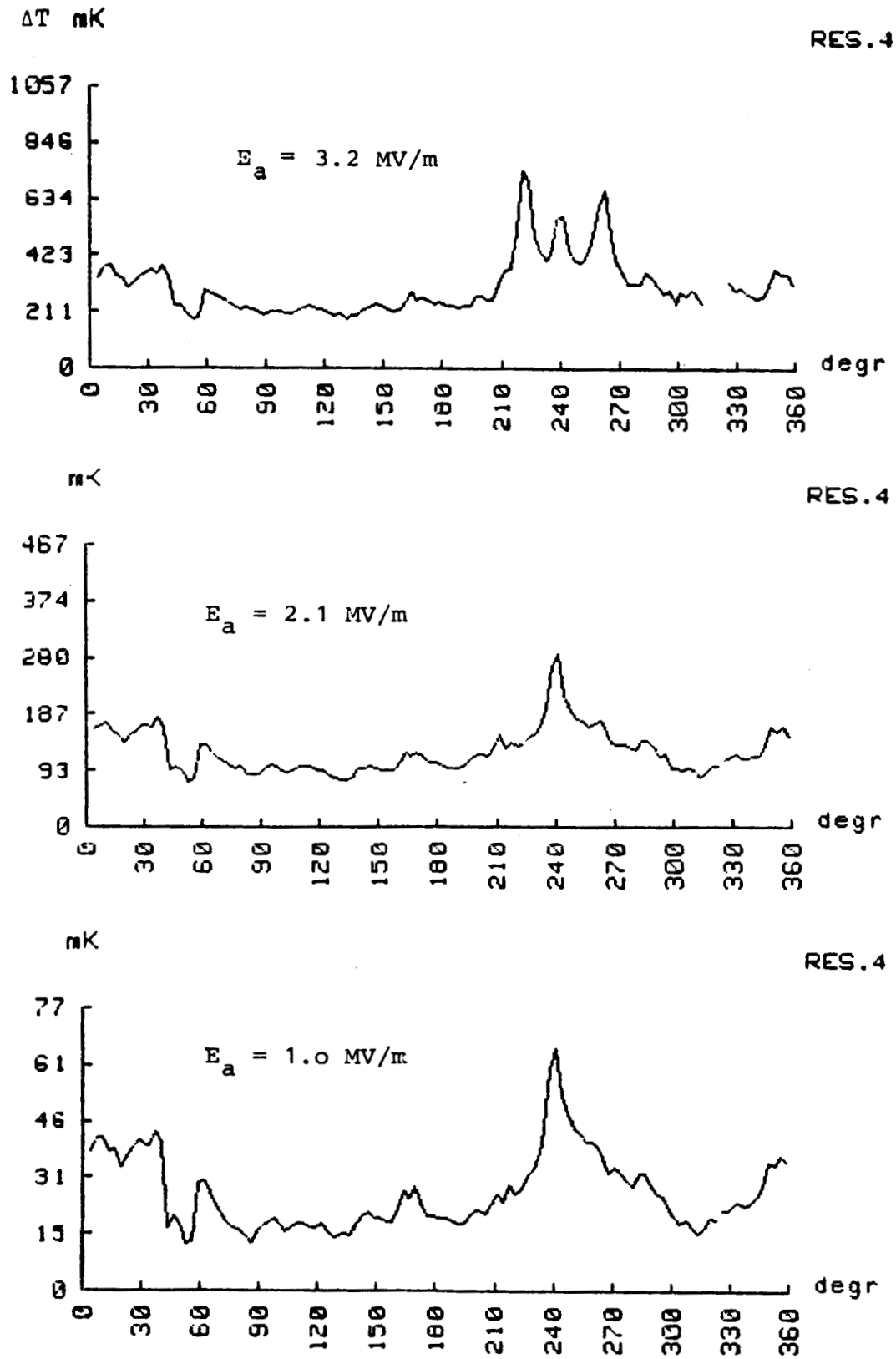


Fig. 24 : Temperature profile measured by resistor 4 along its path around the cavity for three different accelerator fields $E_a$.

Fig. 25 shows a temperature map at a field level ($E_a$ = 3.2 MV/m) where electron loading already is a significant energy loss mechanism. One recognizes the line like loss regions produced by impacting electrons field emitted by point sources which since long have been assumed to exist.

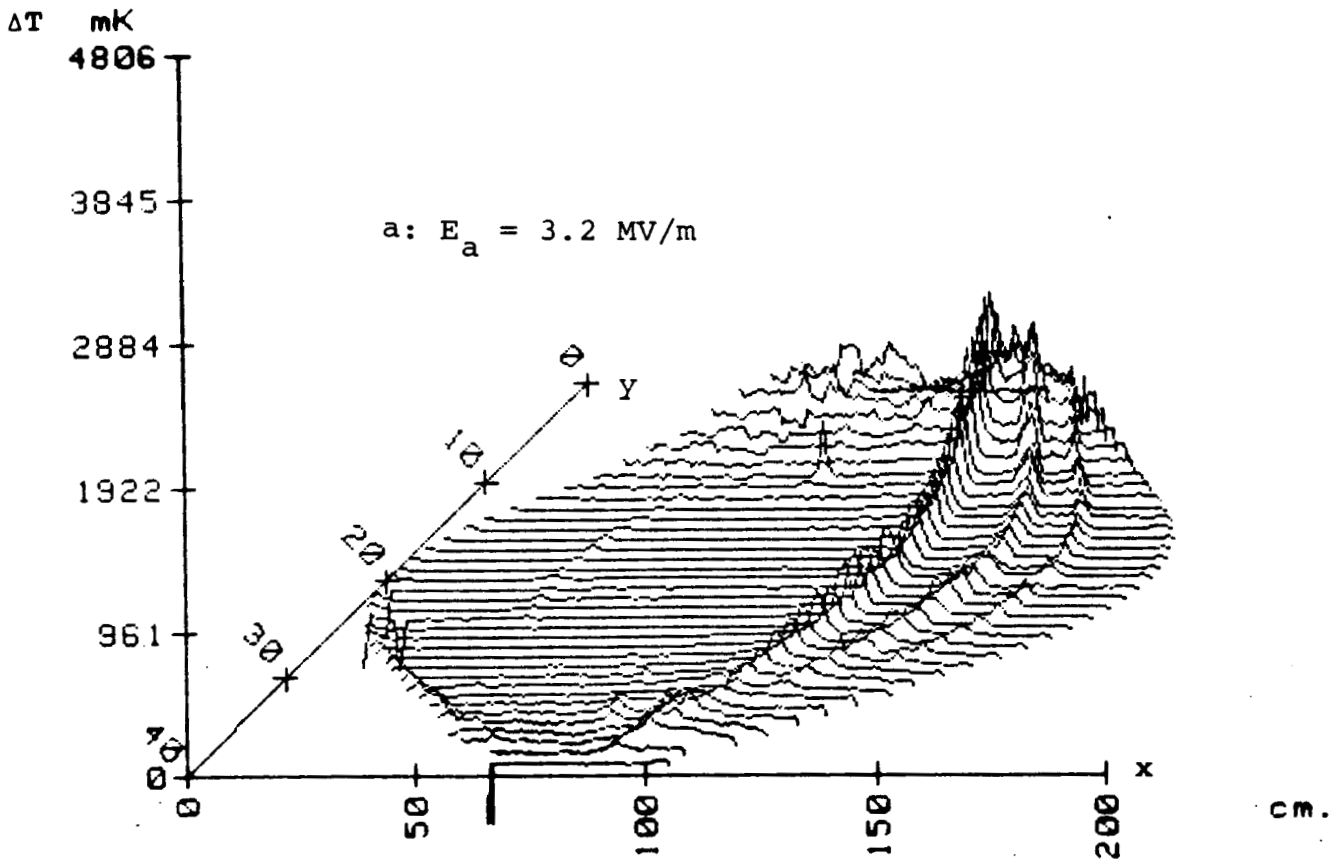


Fig. 25: Temperature map of the CERN 5oo MHz cavity at $E_a$ = 3.2 MV/m with line like regions of increased temperature due to the impact of electrons field emitted by point sources.

During the same experiment but after some intense electron processing at high fields ($E_a \simeq$ 5.2 MV/m) a quench was observed which manifests itself in the map of fig. 26.

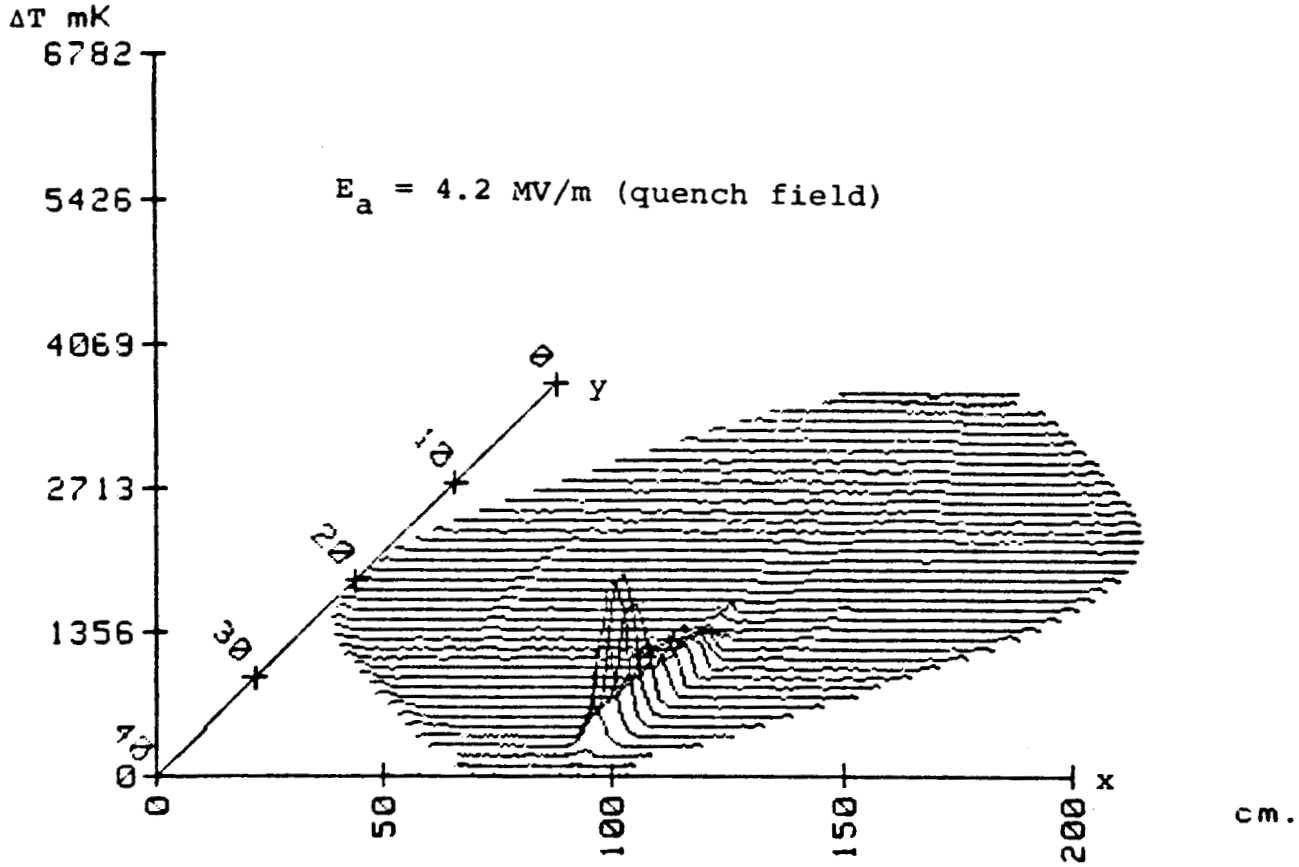


Fig. 26: Temperature map taken during quenching ($U_t$ signal like in fig. 8a)

(Because of a single fast quench (see fig. 8a) only the quench area is heated.) This quench was produced by overheating an area of permanent surface damage, which was produced during the electron processing. This can be seen from the map in fig. 27 which shows this damage well below the quench field (compare also fig. 22 where this damage is not yet present). The electron beam however which produced this damage is not present in fig. 25. The electron processing however which produced the quench was done at a much higher field. The damage causing beam did return after a glow discharge cleaning of the cavity (2).

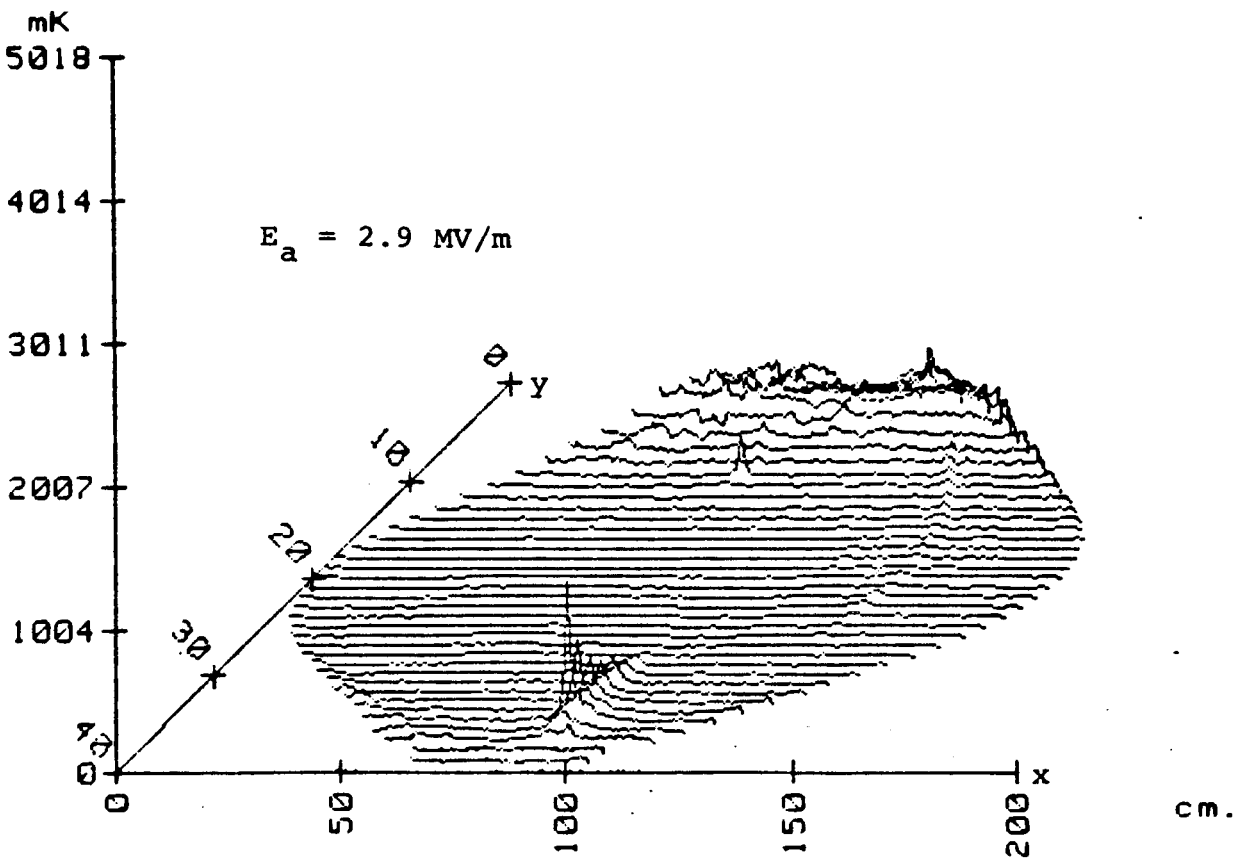


Fig. 27: Temperature map of the 5oo MHz cavity below the quench field.

The discharge cleaning which effects only a very thin surface layer (< 1oo Å thick) did reduce the residual resistance down to 8o nΩ mainly by cleaning the upper part of the cavity. This can be seen from the map of fig. 27 taken after the glow discharge (please note the change of the temperature scale).

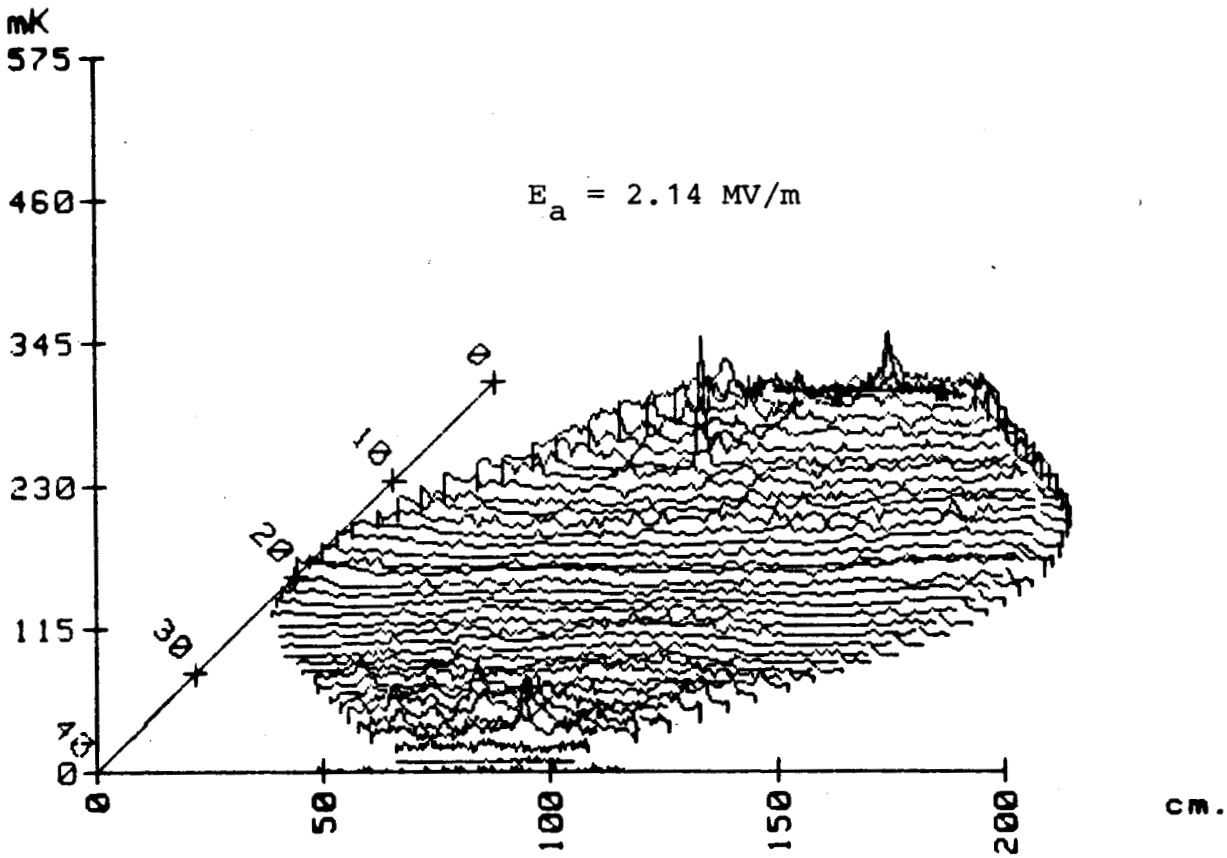


Fig. 28: Temperature map after a glow discharge cleaning at $E_a$ = 2.14 MV/m

The spike resistor 1o (arrow in figs. 27 and 28) which was not reduced by the argon discharge is a nice example of a normal conducting spot which is thermally stable up to high fields.

Another important observation is that the surface damage by electron bombardment is removed. From this one concludes that this type of damage effects only a very shallow surface layer (less than 1oo Å thick). This narrows in the thickness of the damage, compared to earlier experiments at Cornell. After the glow discharge cleaning the cavity also was found highly sensibilized in respect to electron field emission.

In a temperature map taken at $E_a$ = 3.4 MV/m (fig. 29) one can now clearly see the electron impact line which produced

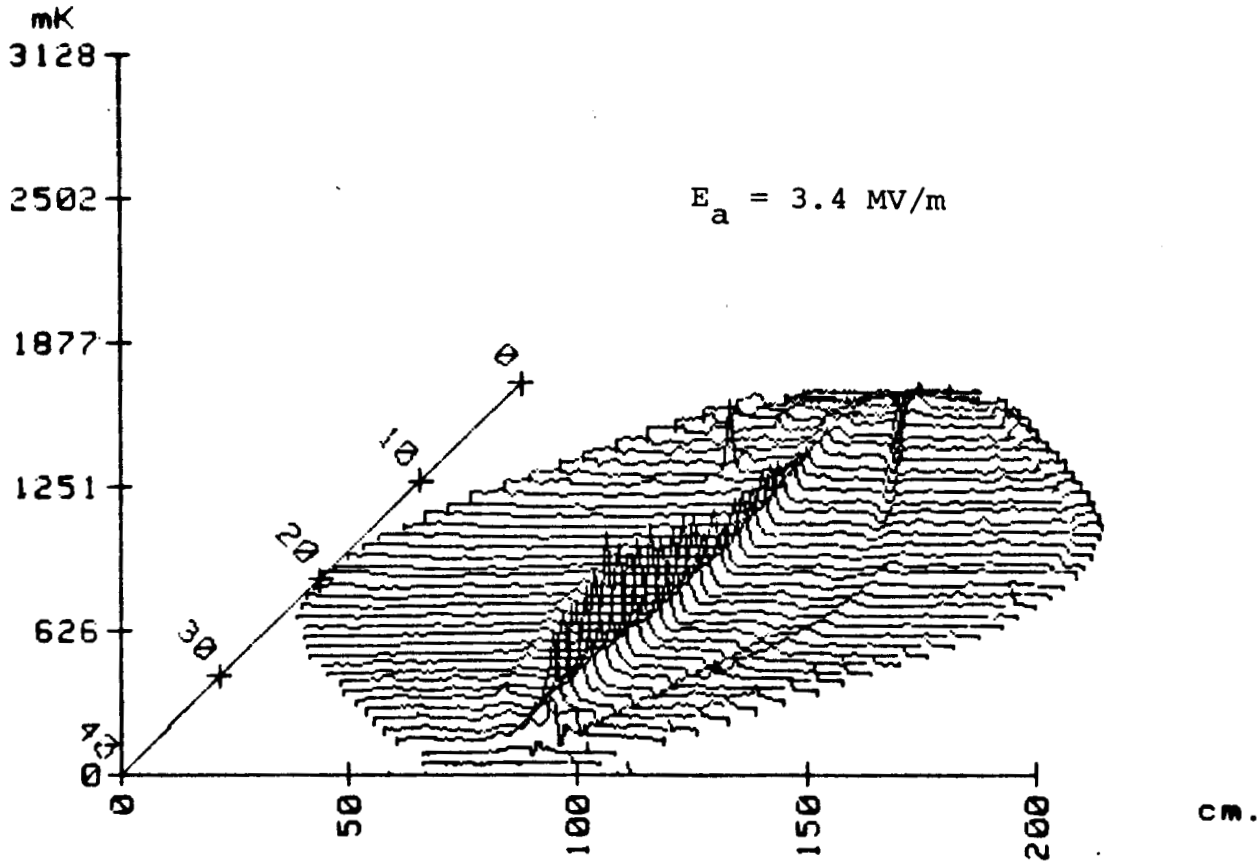


Fig. 29: Strong surface heating by an impacting electron beam considered to be responsible for the surface damage shown in fig. 27.

the damage shown in fig. 27. The production of an invisible surface damage by electron impact has been observed earlier [1o]. The temperature maps shown here confirm these findings in a truly visible form.

Temperature mapping of a superconducting cavity in subcooled helium is just in its infancy. The data analysis at CERN has just started and many more experimental observations are to be expected.

## 5. CONCLUDING REMARKS

A large number of diagnostic techniques has been developed in the past ten years by which we have gained considerable insight into the energy loss mechanism present in a superconducting cavity. Some of the techniques are applicable to practically all cavity shapes. This is true in particular for the observation of the rf signal emitted from the cavity, the detection of breakdown locations with carbon resistors, the measurement of intensity, energy and spatial distribution of X-radiation by NaJ detectors and the detection of internal electron currents by probes in almost field free regions of the cavity. Other more powerful methods can be applied only to cavities of simple shape, like the scanning X-ray detectors and temperature mapping carbon thermometers. These latter techniques however, may teach us how to interpret on save grounds the informations collected by the more easy and more general to use diagnostic procedures.

## ACKNOWLEDGEMENTS

I am very thankful to U. Klein and H. Lengeler for their help and corrections in the course of preparing this review. Indispensible were also the extensive informations and written comments of many representatives of institutions working in this field: K.W. Sheppard of Argonne, H. Padamsee of Cornell, A. Schwettman of Stanford HEPL, P. Kneisel of the Kernforschungszentrum Karlsruhe, Nguyen Tuong Viet of Orsay, H. Pfister of Siemens AG. and G.A.Loew of SLAC.

REFERENCES

1. J. Halbritter, private communication

2. M. Tigner, IEEE Trans.Mag-15,(1978)

3. C.M. Lyneis, P. Kneisel, O. Stolz, J. Halbritter IEEE Trans. Mag-11, No.2, p.417(1975)

4. Ph.Bernard, G.Cavallari, E.Chiaveri, E.Haebel, H.Heinrichs, H.Lengeler, E.Picasso, V.Picciarelli and H.Piel, contribution to the 198o Conference on High Energy Particle Accelerators, Geneva (198o)

5. A. Denitz and H. Padamsee, CLNS-434, Cornell University (1979)

6. C.M. Lyneis,"Electron loading" review talk given at this workshop

7. J. Kirchgessner, H. Padamsee, H.L. Phillips, D.Rice, R. Sundelin, M. Tigner and E. Borstel, IEEE Trans. NS-22, No.3, p.1141 (1975)

8. W. Bauer, A. Citron, G. Dammertz, M. Grundner, L. Husson, H. Lengeler, E. Rathgeber, IEEE Trans. NS-22, No. 3, p. 1144(1975)

9. J. Halbritter, private communication

1o. J.N. Weaver, H. Schwarz, T.I. Smith and P.B. Wilson, HEPL-PC-1 (1968) Stanford University

11. J. Halbritter, Part.Acc. Vol. 3, p.163 (1972)

12. A. Septier, "Surface Studies", review talk given at this workshop.

13. H.A.Schwettman, Stanford University, private communication

14. C.M. Lyneis, H.A. Schwettman and J.P.Turneaure, Appl. Phys. Lett. 31, p. 541 (1977)

15. U. Klein and D. Proch, Proc. of the "Conference on Future Possibilities of Electron Accelerators" Charlottesville 1979

16. H. Padamsee, D. Proch, P. Kneisel and J. Mioduszewski, contribution to the conference on Applied Superconductivity 1980, Santa Fé, Oct. 1980

17. K. Yoshida, M. Yoshioka, J. Halbritter
IEEE Trans NS-26, No. 3 (1979)

18. I. Ben Zvi, J.E. Crawford and J. P. Turneaure
IEEE Trans. NS-20, No. 3, p.54 (1975)

19. K.A. Schwettman, J.P. Turneaure and R.F. Waites,
Journ. of Appl. Phys. Vol.45, No. 2, p. 914 (1974)

20. H. Heinrichs,CERN, private communication (1980)

21. U. Klein, University of Wuppertal and H. Padamsee,
Cornell University - private communications

22. Nguyen Tuong Viet, Orsay, private communication

23. C.M. Lyneis , M. McAshan and Nguyen Tuong Viet,
Proc. of 1972 Proton Linear Acc. Conf. (Los Alamos, 1972)
p. 98.

24. H. Padamsee, J. Kirchgessner, M. Tigner, R. Sundelin,
M. Banner, J. Stimmel and H.L. Phillips, CLNS-340,
Cornell University (1976)

25. H. Piel, R. Romijn, CERN, private communication

26. K.W. Shepard, C.H. Scheibelhut, R. Benaroya and L.H. Bollinger
IEEE Trans. NS-24, No. 3, p.1147 (1977)

27. K.W. Shepard, Argonne National Lab., private communication

28. G. Dammertz, L. Husson, H. Lengeler and F. Rathgeber,
Nucl. Inst. and Meth. 118, p. 141 (1974)

29. U. Klein, D. Proch and H. Lengeler, WU B 80 -16 (1980)
University of Wuppertal

30. Ph.Bernard, G.Cavallari and E.Chiaveri, private communication